Evaluation of the Microstructure, Mechanical and Tribological Properties of Nickel-Diamond Nanocomposite Coatings

E. J. Ekoi [a*] and D. P. Dowling [a]

**Corresponding author:*
University College Dublin, School of Mechanical and Materials Engineering, Belfield, Dublin 4, Ireland
Email: emmanuel.ekoi@ucdconnect.ie

[a] *University College Dublin, School of Mechanical and Materials Engineering, Belfield, Dublin 4, Ireland*
Email: denis.dowling@ucd.ie

Abstract: This study investigates the feasibility of a two-step process for the deposition of wear resistant, nickel-diamond nanocomposite coatings onto steel substrates. The steps involve the spray deposition onto stainless steel substrates, of nickel nanoparticles (40 - 60 nm diameter) and nanodiamonds (approx. 100 nm diameter). This is followed by the sintering of the nanoparticle coating using a microwave plasma. The 0.2 - 2 µm thick nanocomposite coatings exhibited very good adhesion on the steel substrates, based on Rockwell C indentation tests. The morphology and roughness of the coatings was found to be significantly influenced by the sintering temperature, which was investigated in the range 711 to 885 °C. The effect of nanodiamond concentration and spray duration were also investigated. Of the parameters studied, the concentration of nanodiamond in the composite was the dominant factor controlling the wear performance of the coatings, when assessed based on pin-on-disc wear tests. Compared to the nickel coating and the steel substrate, the nickel-diamond nanocomposite coatings exhibited a 126 and 55-fold enhancement respectively, in wear performance.

Keywords: Nanocomposite coating; Spray deposition; Nanodiamond; Microwave plasma; Microstructure; Tribology.

1. Introduction

A number of authors have demonstrated that the incorporation of hard particles into metallic coatings can yield an enhancement in wear resistance compared with that obtained only with the metal only layer [1–10]. For example, Gül, *et al.* [4] reported a two-fold enhancement wear resistance with the addition of SiC particles (0.1 - 1 μm) into a nickel coating. It was highlighted that the enhanced wear performance was due to the dispersion strengthening effect of these particles, which impeded dislocations movement in the nickel matrix [4,11]. Compared to other types of particle reinforcement, diamond is of particular interest, due to its hardness and wear resistance [2,7]. Wang *et. al.* [7] and Petrova *et. al.* [12], both reported that diamond particle (2 – 110 μm) incorporation into a nickel matrix using electroless deposition technique, yielded enhanced wear resistance. A similar study was carried out on Ni-P-C composite coatings, into which diamond particles were added [13]. It was found that the incorporation of smaller diamonds with mean diameters of 3 – 6 μm, exhibited superior wear resistance compared with that obtained for 20 – 40 μm diamonds. A further improvement has been reported by incorporating nanodiamond particles into the metal matrix [10,14,15]. These particles can be synthesised commercially using detonation or high-pressure-high temperature (HPHT) technique [16,17]. Wang, *et al.* [10] for example, prepared nanocrystalline Ni based composite coatings by incorporating nanodiamond particles (10 nm), obtained using electrodeposition. These exhibited a wear rate of approximately 1.4 $x10^{-4}$ mm^3/Nm, compared with 2.5 $x10^{-4}$ mm^3/Nm for the nickel only layer. It is common practice to deposit a nickel coating of several micrometre prior to composite deposition, in order to promote adhesion between coating and substrate [2,12].

An alternative approach, which has been demonstrated to be very effective, is the deposition of diamond protective coating onto substrates, such as stainless steel; via the chemical vapour deposition (CVD) route [18–20]. The advantages of CVD diamond protective coatings include high wear resistance and chemical stability, among others [18]. The two major

problems encountered in CVD diamond protective coatings are the high carbon diffusion; and the thermal expansion coefficient (TEC) mismatch between diamond film and stainless steel; which results in graphitisation and stress, respectively [19–23]. To mitigate these problems, it is essential to deposit an interlayer between diamond films and the stainless steel to act as both a diffusion barrier and a TEC intermediary between diamond films and stainless steel [19,20,22–24]. However, the preparation of diamond films on stainless steel is still a challenge because it is possible for diamond films to delaminate even with the use of interlayers, such as CrN, Cr/Al and Ti/Al [19,25].

In this study the use of a spray deposition technique is investigated in which the metal nanoparticles and nanodiamonds are deposited from a suspension of this particle mixture in an organic solvent. The as deposited, loosely bound nanoparticles on steel substrates, are then sintered in a microwave plasma discharge. This approach has been used previously for the preparation of both TiO_2 and NiO films for use in dye-sensitised solar cells [26–28]. In this investigation this spray deposition technique followed by microwave plasma sintering, is evaluated for the first time for the application of nickel-diamond nanocomposite protective coatings. The effect of sintering temperature, spray duration and nanodiamond concentration on the morphology, surface roughness, thickness, wear rate and adhesion of the nanocomposite coatings are evaluated.

2. Materials and Methods

2.1 Substrate Material and Preparation

Stainless steel 18: 8 (Cr:Ni) discs, of diameter 25 mm and thickness 6 mm were used as test substrates. The discs were ground and polished to a mirror finish using silicon carbide abrasive paper (grit sizes of 240, 320, 360 and 600), diamond suspension (6 and 3 μm) and colloidal silica. Prior to coating, the steel test coupons were cleaned in an ultrasonic bath

using methanol and deionised water; blow-dried with air. The resulting test substrates exhibited a roughness (S_a) of 0.01 μm.

2.2 Suspension Materials and Preparation

Nickel nanoparticles (40 - 60 nm) and nanodiamonds ND (100 nm) of HPHT origin were obtained from Skyspring Nanomaterials, Inc. and Shannon Abrasives Ltd, respectively. These were mixed with a solvent and sonicated in an ultrasonic bath for 30 minutes prior to spraying onto the steel substrate. The suspensions were prepared by mixing various ratios of 0.399 g of nickel-diamond nanoparticle powder with 40 ml of Isopropanol (IPA) from Sigma Aldrich Ltd.

2.3 Spray Deposition Coating and Sintering Processes

Prior to the deposition process, the suspension was left to stand for five minutes after sonication. Spray deposition of the nanoparticle layer was carried out using the following components: an AutoGrav 3-Achsen CNC system, a spray unit which comprised a Burgener nebuliser (Ari Mist HP), a liquid delivery syringe (SEG 10 ml); a pump system (Aladdin Single-Syringe Pump) from World Precision Instruments (WPI); and a heating system for substrate heating prior to deposition. The distance between the nebuliser tip to the substrate was fixed at 15 mm and the nebuliser scanned across the substrate at a speed of 10 mms^{-1}, with a step interval of 1 mm during the deposition process. Nitrogen operating at 0.552 MPa was used as the nebulising gas and the suspension flow rate was maintained at 30 μl/min by the pump system. The region to be coated on the substrate was determined by masking with a scotch tape (3M). This also enabled the measurement of coating thickness. Prior to nickel-diamond nanoparticle deposition, the masked substrate was mounted on a heated bed and left for five minutes in order to maintain the substrate temperature at 50 ^{o}C. The heating system was used to aid in the evaporation of the organic solvent during deposition, to avoid solvent build-up. The deposited particles were sintered using a microwave Circumferential Antenna

Plasma (CAP) reactor, as described previously [29]. This hydrogen-nitrogen discharge operated at a pressure of 1.9 kPa, and frequency of 2.45 GHz. A sintering time of 3 minutes was used for each sample treatment. Temperature measurements during sintering were carried out using an LPC03 ratio pyrometer from Dr. Mergenthaler GmbH & Co. KG, which has an accuracy of +/- 2 °C in the temperature range investigated. The temperature generated on the steel substrate by the discharge was found to be in the range of 707 ± 25 to 901 ± 28°C, depending on the microwave plasma processing conditions used. These measurements are the average of the three sample measurements obtained at each treatment temperature.

Three parameters were investigated namely: the effect of sintering temperature, nanodiamond concentration and the spray duration (a function of number of passes). The experimental conditions are presented in Table 1. A minimum of 3 tests were carried out for each data point investigated. Coating performance was evaluated based on its morphology, roughness, thickness, adhesion and wear resistance.

Table 1: Spray deposition and sintering conditions investigated.

	Effect of Technological Parameters		
	Nanodiamond Concentration	Spray Duration	Sintering Temperature
% Nanodiamond Concentration (wt%)	0 - 25	15	15
Suspension Concentration ($x10^{-3}$) (g/mL)	9.98	9.98	9.98
Suspension Flow Rate (µL/min.)	30	30	30
Spray Duration (Minutes)	90	30 - 150	90
Sintering Temperature (^{o}C)	812	812	710 - 885

2.4 Material Characterisation

The morphology of the composite coatings was characterised using FEI Quanta 3D FEG DualBeam and Hitachi SU8230 scanning electron microscopes (SEM); and a FEI Tecnai F30

Twin transmission electron microscope (TEM). Cross-section analysis of the coating was obtained using a focused ion beam (FIB). To facilitate obtaining the FIB cross-sections, a 2 × 30 μm, 1 μm thick Platinum (Pt) layer was deposited on the surface. A 30 kV ion beam at a current of 15 nA was used to cut the initial cross-section in the material; the cross-section surface was subsequently cleaned at 1 nA and 0.1 nA. Energy-dispersive X-ray spectroscopy (EDX) was used to obtain elemental data. Coating roughness (S_a) and thickness were measured using both a Bruker's NT1100 and NPFLEX 3D optical profilometers in vertical scanning interferometry (VSI) mode. The phase composition and crystallinity were determined using Siemens D500 XRD and inVia Micro-Raman confocal spectroscopy system (Renishaw, Wotton-under-Edge, Gloucestershire, UK). The XRD system operated at 40 kV and 30 mA at a wavelength of 0.1541 nm (CuKα radiation). The scan wavelength for this system was in 2θ mode with a scanning range from 10° to 100° with steps of 0.02° per second. Raman scattering was recorded using a laser of wavelength 532 nm with a maximum laser power of 4.5 W. A 10x objective lens was used to focus the laser beam on the sample surface for an exposure time of 10 seconds each time. Spectra were calibrated to a silicon shift at 520 cm^{-1}. The detector used was a NIR enhanced Deep Depletion CCD array (1024 × 256 pixels) which was Peltier cooled to -70°C. A 1800 lines/mm grating was used for all the Raman scans. Point spectra were obtained using the "Extended" scan option in this system, resulting in spectra in the Raman shift range of 20 - 3202 cm^{-1}.

The wear performance of the deposited coatings was assessed using a POD-2 pin-on-disc system (Teer Coatings Ltd., UK), operating at room temperature under dry condition. The temperature and humidity were 21 ± 2 °C and 44 ± 5 %, respectively. A WC-Co ball with a diameter of 5 mm was used as a counterpart under a constant load of 1 N. The disc rotated at a speed of 96 RPM (equivalent to a linear speed of 30 mms^{-1}) and a track diameter of 7 mm. Coating/ ball wear track/ scar profiles were obtained using optical profilometry; and the material volume loss calculated according to the ASTM-G99 standard [30]. The adhesion of

nickel-diamond nanocomposite coatings was evaluated using a Rockwell C test method, using an Indentec Hardness Tester operating at a load of 1471 N using a 120^{o} conical diamond indenter. Four indents per sample was carried out and the adhesion strength quality classification determined based on the VDI 3198 guidelines using a Hitachi (TM-1000) Scanning Electron Microscope (SEM).

3. Results and Discussion

In order to optimise the performance of the deposited coatings the following parameters were evaluated - microwave plasma sintering temperature, spray duration and nanodiamond concentration. An initial investigation was carried out to confirm the retention of the nanodiamond particles in the spray deposited and sintered coatings. The coating adhesion was also investigated using Rockwell C. Figure 1 shows the morphology of the nanodiamonds and the nickel nanoparticles used in this study. The average crystallite size of the nanodiamonds and nickel nanoparticles, as estimated using the Scherrer technique, were 33 and 54 nm, respectively. The XRD profiles of the two powders are given as supplementary information (S1).

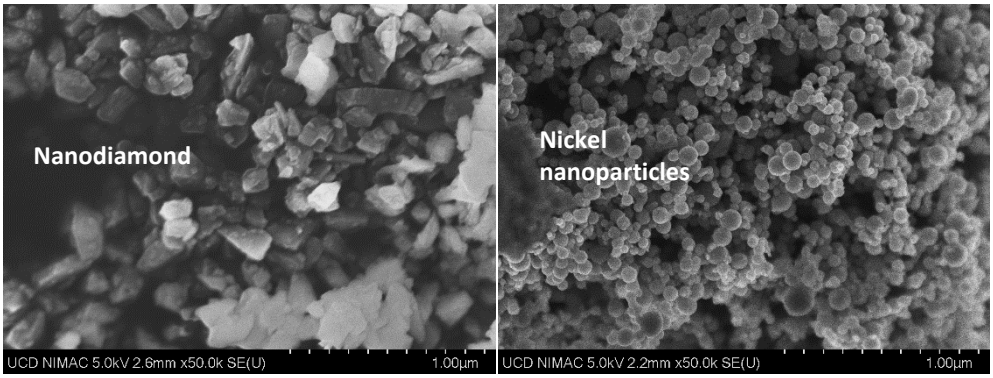

Figure 1: SEM images of the morphology of nanodiamonds and nickel nanoparticles. Scale bar 1 µm.

3.1 Effect of Nanodiamond Concentration

The starting point of this study is to investigate the stability of nanoparticles in alcohol suspension. The stability of nanodiamond in suspensions is significantly influenced by the adsorption of organic molecules on the nanoparticles, by Coulomb interactions, electrostatic or non-electrostatic mechanisms; and has been reported to be dependent on temperature, pH and concentration of the stabilising agent [31–35]. A preliminary investigation carried out during this study on nickel and nickel-diamond nanoparticle suspension in isopropanol (IPA) and methanol showed that the nanoparticles did not agglomerate and/ or settle quickly in isopropanol but did in methanol. A possible reason for this difference is that for nanodiamond dispersions in IPA and methanol, the associated zeta potential values are reported to be +39 and +25, respectively [34]. In this work, IPA was used as the stabilising agent and repeat experiment showed that nickel-diamond nanoparticle suspensions containing 5 to 10% nanodiamond particles were found to agglomerate and settle to the base of the container, in approximately 30 minutes. At higher concentrations, however, the nickel-diamond nanoparticle suspension was found to be stable and was observed to remain so for several months.

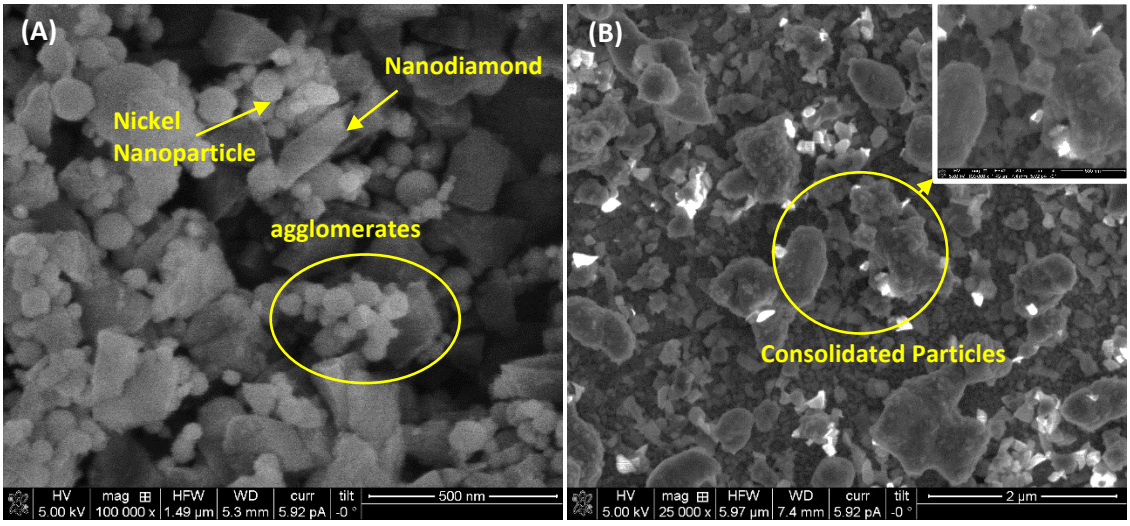

Figure 2: Comparison of the morphology of as-deposited and sintered coatings with 15% nanodiamond concentration: (A) The as-deposited nanocomposite exhibited agglomeration of particles, while these were found to consolidate in the case of the sintered composite (B). Scale bar for A, B & inset 0.5, 2 & 0.5 µm, respectively.

Having identified that suspension concentrations with a minimum of 15% nanodiamond concentration is required to yield a homogenous nanocomposite coating, the next issue evaluated was the morphology of the as-deposited and sintered coatings. The SEM image given in Fig. 2 (A) shows the presence of nanoparticle agglomerates in the as-deposited coatings. These appear to be agglomerates of nickel nanoparticles around those of nanodiamond. The agglomerated nickel nanoparticles melted and formed sub-micron-scale consolidated particles upon sintering. The sizes of these consolidated particles appeared to be influenced by the nanodiamond concentration. As the nanodiamond concentration was increased from 15 to 20% the sizes of these consolidated particles decreased from 0.95 ± 0.21 to 0.73 ± 0.18 µm. A further feature of note is the highly porous nature of the composite structure (Fig. 3). Visual examination indicated an apparent reduction in porosity as the nanodiamond concentration in the spray increased. The relatively homogeneous distribution of porosity in the structure could be attributed to the spray deposition method. The porous nature of spray-deposited / sintered metal oxide coatings has been reported previously [26–28].

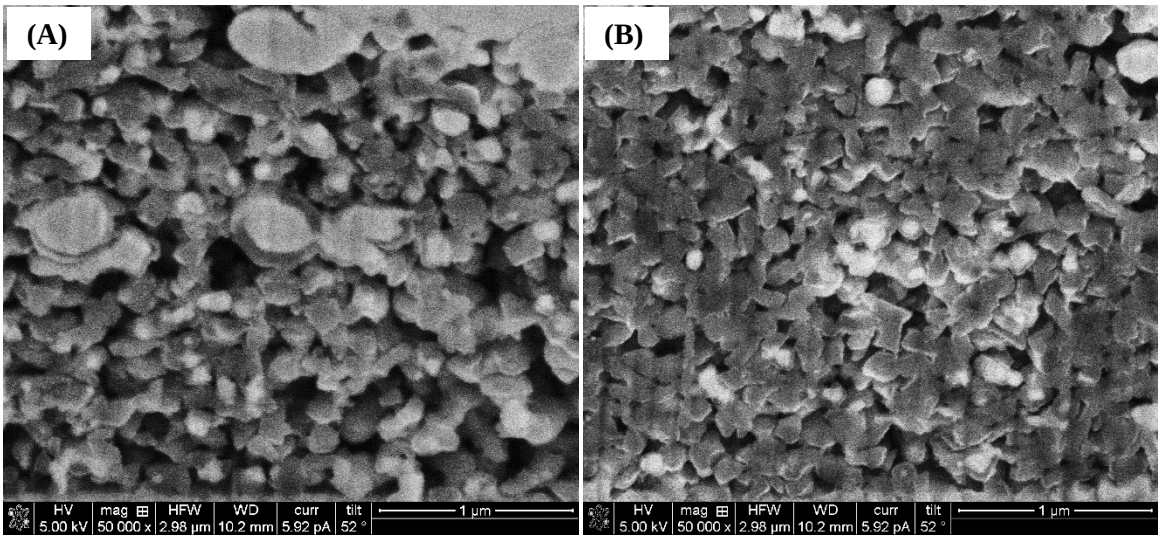

Figure 3: FIB cross-sections of typical nickel-diamond nanocomposite coatings showing their highly porous structure. The samples were deposited from: (A) 20% & (B) 25% nanodiamond concentrations. Scale bar 1 µm.

In this study, all the spray deposition experiments were carried out over a 90-minute period. An investigation was carried out to determine how the concentration of nanodiamond used in the suspension influenced the surface roughness (S_a) and thickness of the coatings obtained after sintering. The results of this study are given in Fig 4. This demonstrates that at low nanodiamond concentrations, very thin layer coatings are deposited. Above 15% nanodiamond concentration, however, there is an increase in both the average surface roughness and coating thickness, as thicker layers were deposited from the nanoparticle / solvent suspension.

Considering the original particle size and shape of the nanodiamonds (ND) (100 nm and irregular (blocky), respectively) shown in Fig. 1 & 2 (A), it is possible that by increasing the nanodiamond concentration in the coating, the level of shrinkage and pore refinement by particle rearrangement and necking during microwave plasma sintering could be influenced by the presence of non-shrinking hard nanodiamond particles.

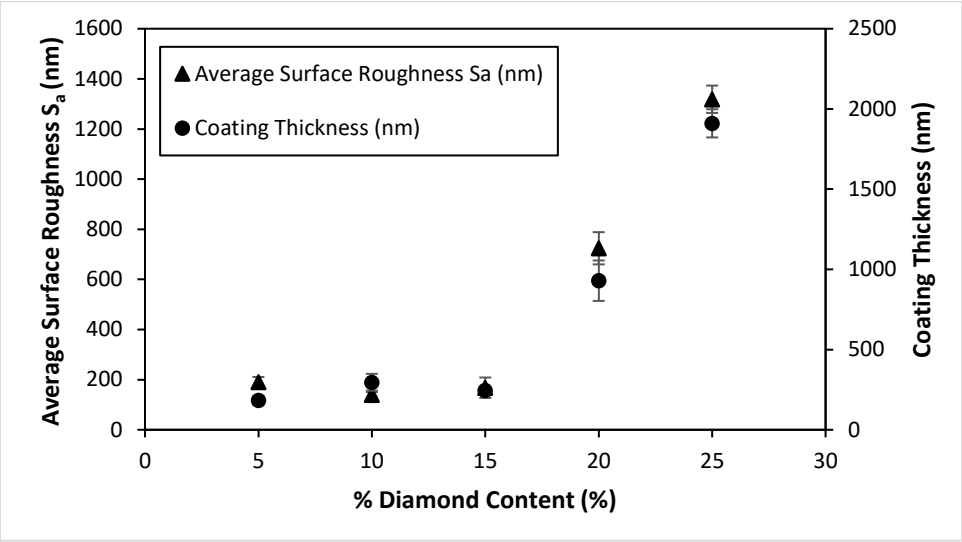

Figure 4: Effect of nanodiamond concentration on the surface roughness (S_a) and thickness of the sintered coatings.

3.2 Effect of Spray Duration

The effect of spray time (dependent on the number of passes of the nebuliser during spray), on the morphology, surface roughness and thickness of coatings sintered at 812 ºC, is evaluated. The thickness of the layer after spraying (prior to sintering) is given in Fig. 5 and shows broadly a linear relationship with spray duration. On examining the coatings after subsequent sintering as shown in Fig. 6, two regimes are observed, firstly for spray durations up to 90 minutes, a high level of densification occurs during sintering. In contrast, after longer spray periods a significant increase in thickness was observed. A possible explanation for this is that for the thinner coatings some particle rearrangement may have occurred facilitating a denser structure.

It is noticeable from Figs. 4, 5 & 6 that there appears to be a broadly linear relationship between coating thickness and roughness. This correlation was further demonstrated when the thickness and roughness of a larger range of nanocomposite coatings independent of experimental conditions were plotted against each other (Fig. 7).

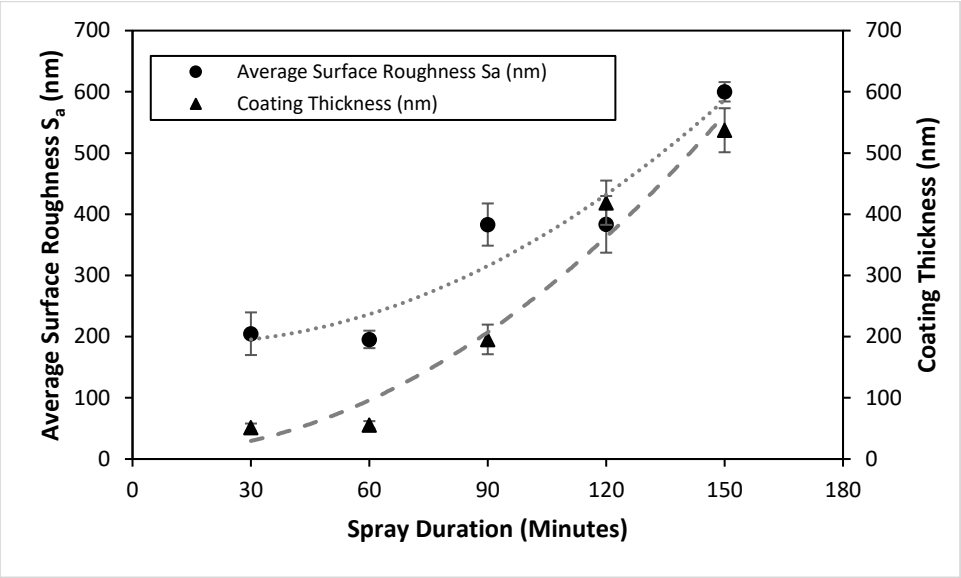

Figure 5: Effect of spray duration on the average surface roughness (S_a) and thickness of as-deposited composite layers, prior to sintering.

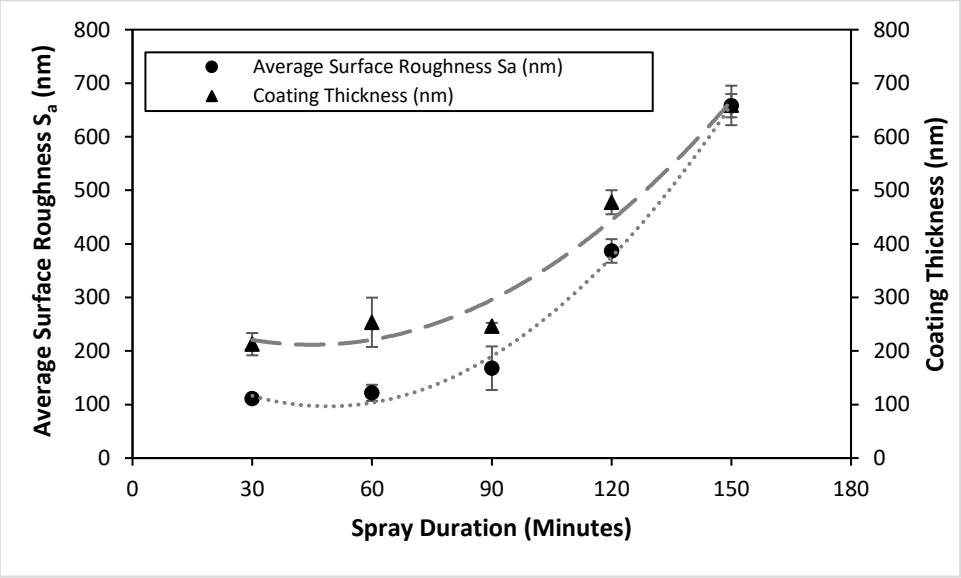

Figure 6: Effect of spray duration on the average surface roughness (S_a) and thickness of the sintered composite coatings.

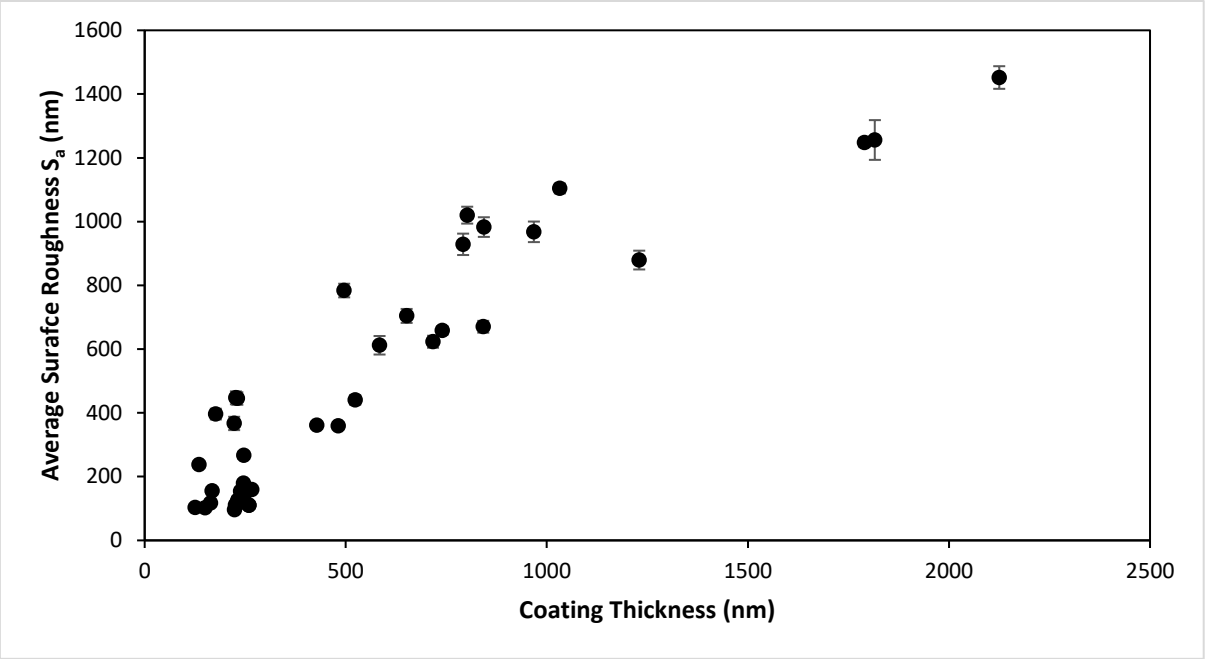

Figure 7: Effect of coating thickness on the average surface roughness (S_a) of nickel-diamond nanocomposites obtained for a range of nanodiamond concentrations and processing conditions.

3.3 Effect of Sintering Temperature

The effect of microwave plasma sintering temperature on the average surface roughness (S_a) and thickness of the nickel-diamond nanocomposites coatings (15% nanodiamond concentration) is shown in Fig. 8. The coating roughness generally decreased with increasing temperature as did its thickness. This effect is associated with the increased densification of the composite coatings at higher sintering temperatures [36]. The effect of temperature on densification can be observed in the TEM images of typical coatings sintered at 711 and 821 ^{o}C, it is noticeable that there was a decrease in pore size with increasing temperature (Fig. 9).

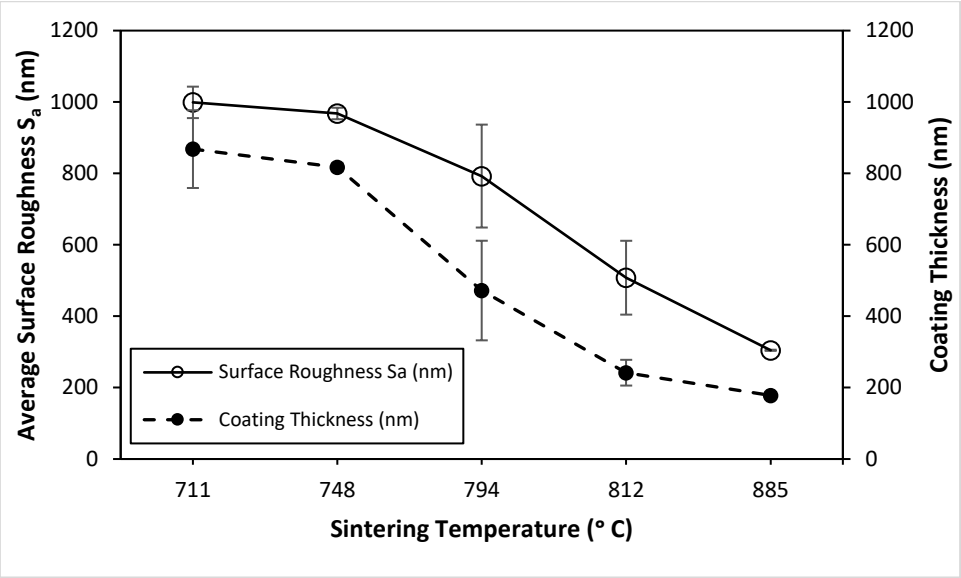

Figure 8: Effect of sintering temperature on the average surface roughness (S_a) and thickness of nickel-diamond nanocomposite coatings containing 15% nanodiamond.

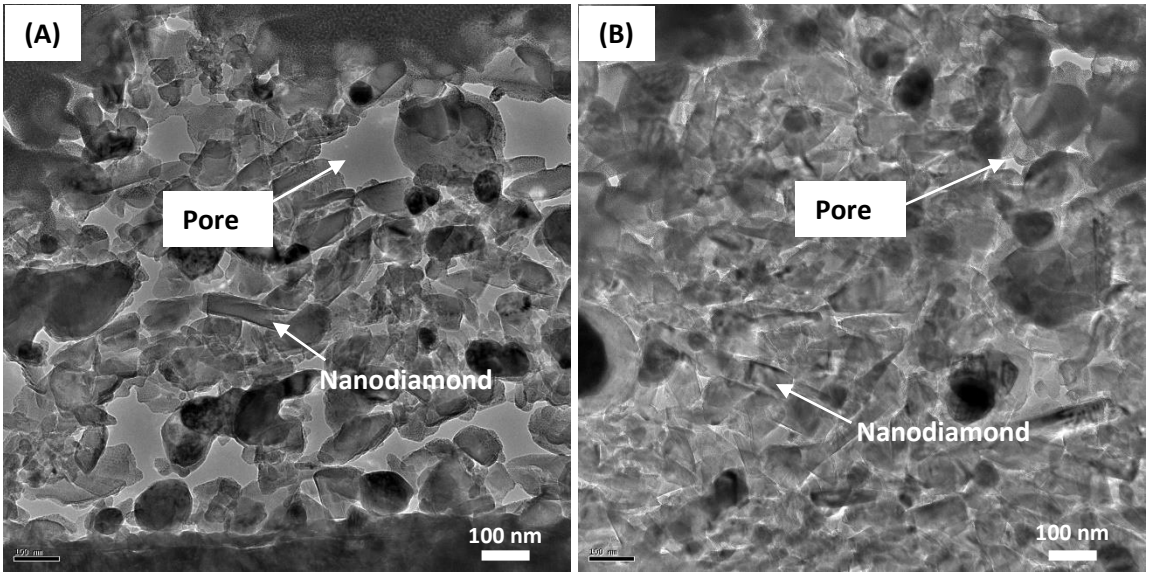

Figure 9: TEM images of the FIB sections of typical nickel-diamond nanocomposite coatings containing 15% nanodiamond concentration and sintered at: (A) 711 & (B) 821 °C. A more highly porous structure is observed in A compared to that observed for B. Scale bar 100 nm.

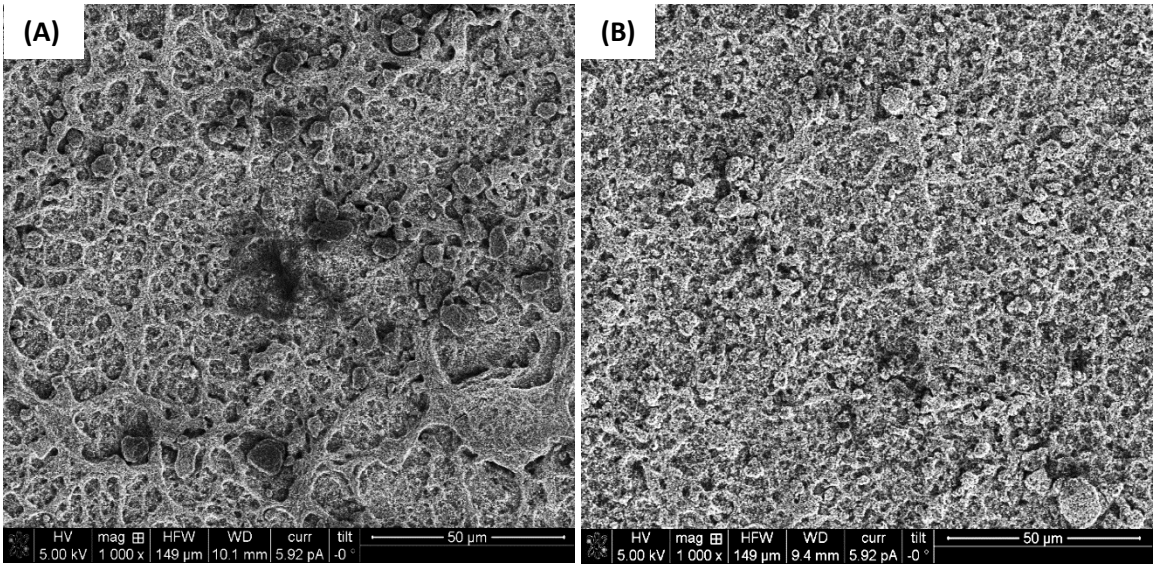

Figure 10: Effect of microwave plasma sintering temperature on the morphology of nickel-diamond nanocomposite coatings: (A) 711 °C; (B) 821 °C. Scale bar 50 µm.

Associated with the change in roughness; as demonstrated in Figure 8, there was a notable change in the morphology of the sintered composite coatings. As shown in Figure 10, the morphology of the coating sintered at 711 °C exhibited a 'fibrous-like' structure which gradually changed to denser, granular structure at the higher sintering temperature (821 °C).

3.4 Nickel-Diamond Nanocomposite Coating Examination by Raman Spectroscopy

The spray deposited and sintered nickel-diamond (15%) nanocomposite coatings appeared homogenous and well adherent based on an initial optical microscopy examination. In order to determine if graphitisation of the nanodiamond had occurred during sintering a Raman spectroscopy examination was carried out. As demonstrated in Figure 11 the observed bands are that of diamond (1328 cm^{-1}) and graphene-like carbon (GLC) (1578 cm^{-1}) [16,37]. A deconvolution of the bands indicated that the diamond band consists of diamond peak (1328 cm^{-1}), which exhibited a small redshift with increasing sintering temperature, as well as overlapping peaks on the shoulder indicating that the diamonds are nanodiamonds [16,37].

The band at 1578 cm^{-1} (consisting of overlapping peaks) and those associated with the diamond band shoulder, is indicative of surface defect modes [16,38], which gradually increased with increasing sintering temperature. The 2D band at 2680 cm^{-1} comprised a single low intensity peak for coatings sintered at 711 ^{o}C; and subsequently developed shoulder peaks, as the sintering temperature increased to 821 ^{o}C, possibly indicating a slight change in structure [38]. It has been reported also that the slight redshift of the diamond line (1328 cm^{-1}) from the natural diamond line (approx. 1332 cm^{-1}) is indicative of the presence of a slight tensile residual stress in the diamond coating and could result in coating debonding [25,39–41]. The potential source of the tensile stress could be the presence of grain boundary, impurity (graphene-like carbon), and vacancy as concluded by Kim and Yu [42] for CVD diamond films. However, the results of the indentation test carried on these coating showed no coating delamination, indicating that the level of stress generated (during deposition and cooling of coatings after sintering), was not enough to cause failure [25].

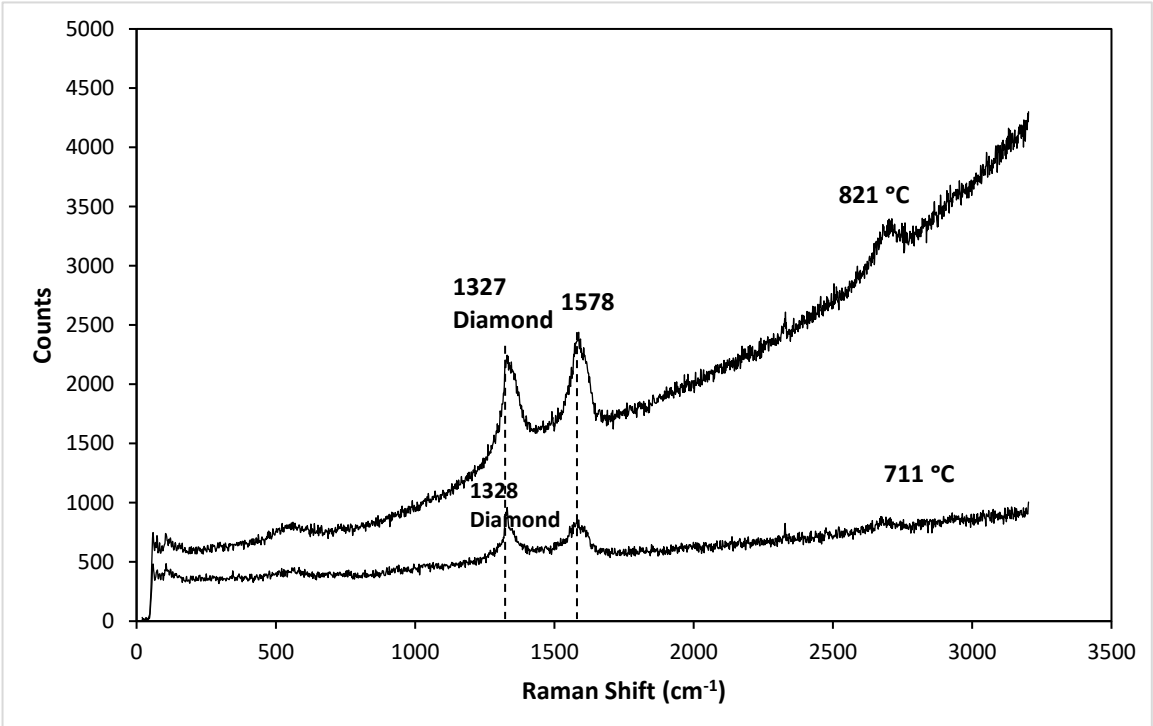

Figure 11: Raman spectra of nanoparticle composite coatings (15 wt% nanodiamond), obtained after sintering at 711 & 821 ^{o}C. Note that the intensity of the diamond and GLC bands increased with increasing sintering temperature.

3.5 Adhesion and Wear Performance of the Nanocomposite Coatings

3.5.1 Adhesion Performance of Nanocomposite Coatings

A Rockwell C indentation test according to the VDI 3198 standard, was used to determine the adhesion of the nanocomposite coatings on the steel substrates [43,44]. It was observed that the microwave plasma sintering temperature, spray deposition time or nanodiamond concentration, was not found to affect coating adhesion; no crack or/and delamination was observed. The adhesion strength quality for the coatings based on VDI 3198 standard was allocated to HF 1. The strong adhesion of the coatings to the steel substrate may be related to the high surface area of the nanometre sized precursor particles, in addition to the nickel matrix, which has a thermal expansion coefficient close to that of stainless steel.

3.5.2 Wear Performance of Nanocomposite coatings

The wear performance evaluation of the nanocomposite coatings was investigated using a pin-on-disc system. The coating after wear testing was evaluated using optical profilometry (Bruker NPFLEX system) as shown in Fig. 12. Addition of nanodiamond to a nickel matrix improved the wear performance significantly. For example, a nickel only coating with thickness of 659 ± 37 nm yielded a wear resistance of (4.3 ± 0.0) x 10^{-4} mm^3/Nm, while that obtained with 15% wt% nanodiamond of the same thickness, was (3.4 ± 0.2) x 10^{-6} mm^3/Nm. The thickness of the test coatings used in the comparison is as given in Fig. 6.

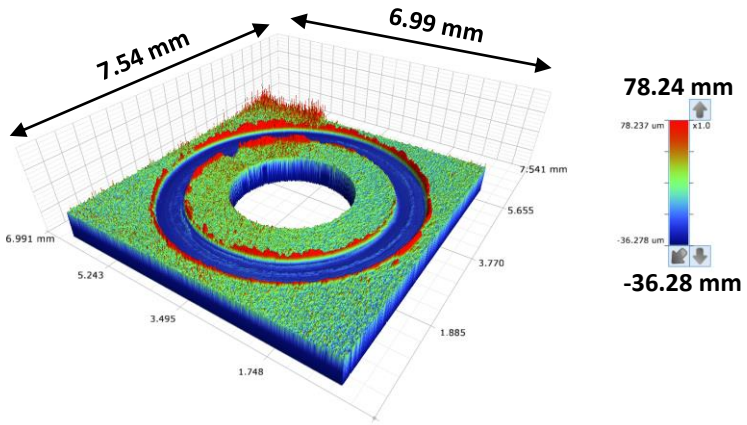

Figure 12: A typical wear track of nanocomposite coatings.

Figure 13 shows the effect of nanodiamond concentration in the range 5 to 25 wt%, on the wear performance of nickel matrix coatings. The thickness of the test coatings is as given in Fig. 4. The increasing nanodiamond concentration yielded a substantial increase in the wear performance. Figure 13 also indicates that the coating obtained with the 5 wt% nanodiamond concentration, was insufficiently robust to withstand shear strain during sliding. Examination of the wear rates in Fig. 13 demonstrates that the 10% nanodiamond coating exhibits a much lower level of wear compared with that obtained for the 15% coatings. It is unlikely that this is due to experimental error as the results as shown are based on a minimum of three test samples per data point. A possible explanation for this behaviour may lie on the kind of reinforcing mechanism in the nickel-matrix nanocomposite (MMnC). This can be due to dispersion and/or particle strengthening mechanisms, which may influence the load bearing capability of the nickel matrix and diamond nanoparticles [45–47].

In addition to the wear observed for the coated steel substrates, it is important to note that as the nanodiamond concentration increased, there was an increased level of wear observed on the pin-on-disc WC balls (Fig. 14). Table 2 compares the wear performance of selected coatings and the associated WC balls, with and without nanodiamond particles. It is clear from this that the level of wear of the WC ball increased significantly as the nanodiamond

concentration increase. For instance, it can be observed that for the 25 wt% nanodiamond sample, the wear of the WC ball was even greater than that of the nanocomposite coatings.

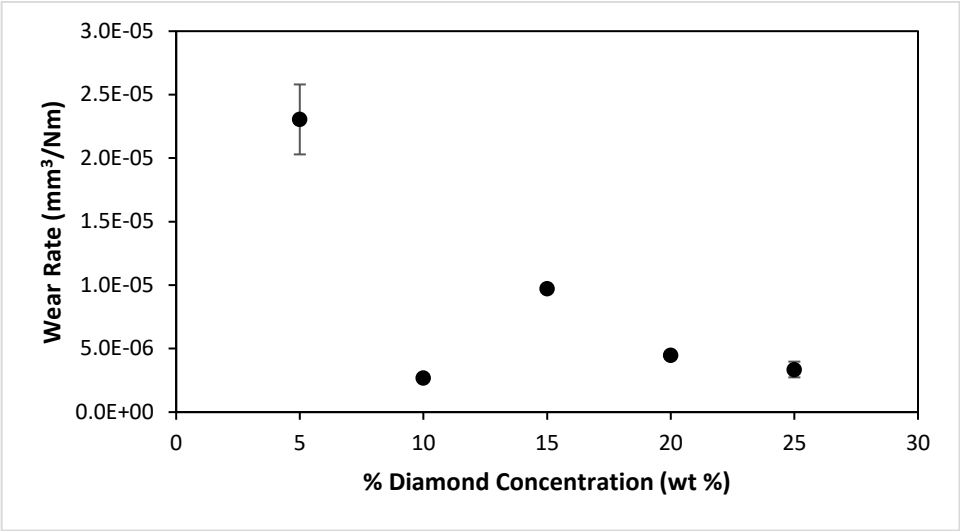

Figure 13: Comparison of the effect of nanodiamond (ND) particle addition on the wear performance of coatings sintered at 812 °C.

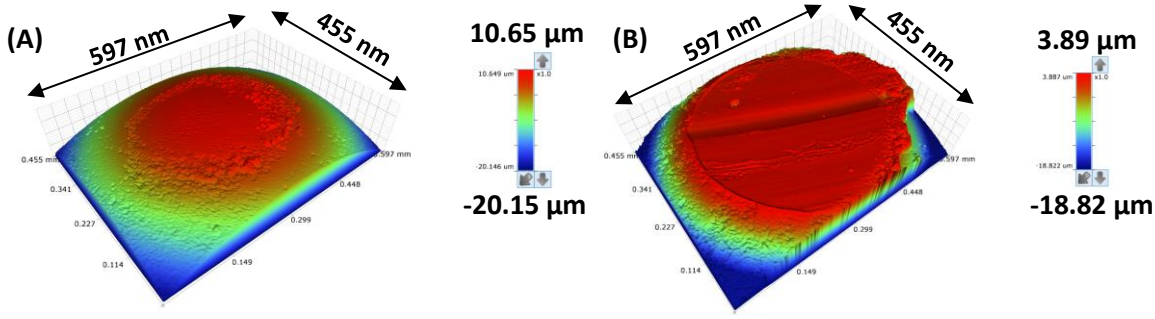

Figure 14: 3D image of the wear scar on the WC balls used for pin-on-disc testing of coatings containing: (A) 5%; (B) 25% nanodiamonds.

Table 2: Wear rate of the nickel coating, along with those containing 5 and and 25 wt% nanodiamond, in addition to the wear rate on the WC balls used for the pin-on-disc testing.

% Nanodiamond Concentration (wt%)	Wear Rate (mm^3/Nm)	
	Coating	Ball
0	$(4.3 \pm 0.0) \times 10^{-4}$	0.0
5	$(2.3 \pm 0.3) \times 10^{-5}$	1.9×10^{-6}
25	$(3.4 \pm 0.6) \times 10^{-6}$	1.2×10^{-5}

A literature study was carried out in an attempt to compare the wear performance of the spray-deposited nickel-diamond nanocomposite coatings with previous studies on nickel-diamond and TiC/a-C nanocomposites. The results of this comparison are given in Table 3. The test conditions used for each of the wear tests are different and thus this comparison can only be considered as semi-quantitative. Nevertheless, it is concluded that the spray deposited coating exhibits superior performance to that obtained by electrodeposition and is similar in performance to the TiC/a-C nanocomposite coatings prepared by sputter deposition.

Table 3: Comparison between the wear performance of coatings obtained in this study and examples quoted from the literature.

	This Study			Wang, *et al.* [10]	Kumar, *et al.* [48]
Material	Steel Substrate	Nickel Coating	Nickel-diamond Nanocomposite	Nickel-diamond Nanocomposite	TiC/a-C Nanocomposite
Deposition Technique	-	Spray Deposition	Spray Deposition	Electrodeposition	Sputter Deposition
Wear Rate (mm^3/Nm)	2.3×10^{-5}	4.3×10^{-4} (sintered)	4.2×10^{-7} (sintered)	5.0×10^{-5}	4.0×10^{-7}

3.5.2.1 Wear mode(s) and mechanism of the nickel-diamond nanocomposite coatings

In order to investigate the wear mode(s) and mechanism(s) involved in the sliding process of the pin-on-disc system, SEM images of the wear surface of a coating (15% nanodiamond concentration) sintered at 711 ^{o}C are presented in Fig. 15. Figure 15 (A) indicates that the wear track is composed of a relatively smooth worn surface containing regions of a material transfer, which has undergone a high level of plastic deformation – an indication of the presence of a very high shear strain [49,50]. Also, debris materials can be found displaced to the side of this wear track. The morphology of the relatively smooth worn surface and the presence of a wear shoulder (light colour region in Fig. 15 (B)), indicates that the surface has been worn by abrasion [49,51]. A delamination and fracture of the regions in high local stress in the transfer layer can be observed in Fig. 15 (A & C). High plastic deformation generally leads to crack initiation, its growth, followed by delamination [52] as shown in Fig. 15 (C). The presence of a worn surface, plastically deformed transfer layer containing microcracks, delamination and fracture surface, and a displaced side debris indicates that the general mode of wear is a combination of abrasive and adhesive wear [53]. The same mode of wear is observed on the wear scar found on the WC balls, the grooved appearance indicates a ploughing action of the nanodiamond particles (Fig. 16). The wear scar diameter of the WC ball used for coatings sintered at 711 ^{o}C and at 821 ^{o}C were similar (Table 4); and indicates that the abrasive wear of the WC balls was more influenced by the nanodiamond concentration in the coating rather than the sintering temperature.

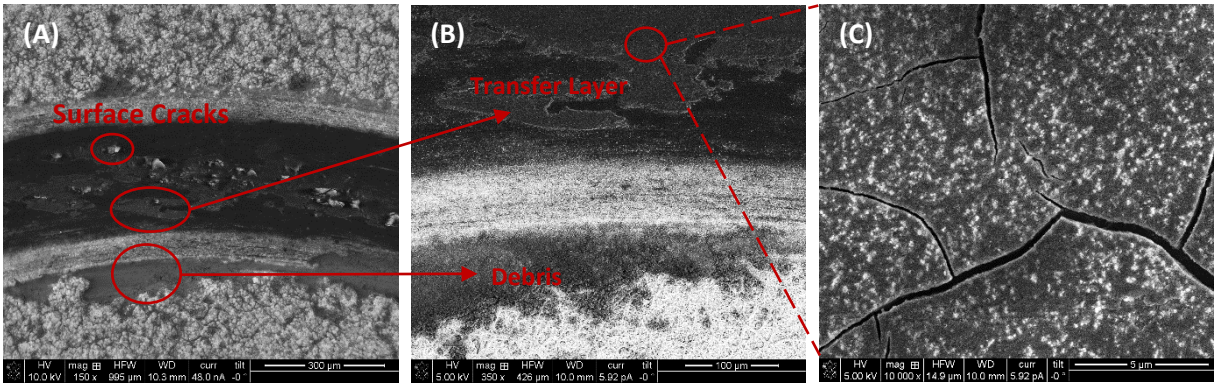

Figure 15: (A) SEM image of the wear track of the nanocomposite coating (Coating sintered at 711 ^{o}C). Within the track, there is a transfer layer from the WC ball (B); (C) A magnified image of microcracks.

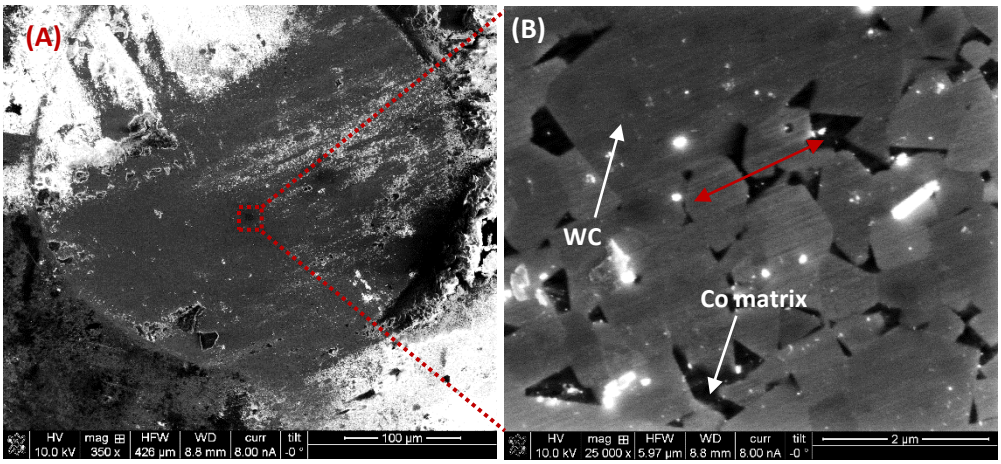

Figure 16: (A) SEM image of the wear scar on the WC balls used for pin on disc measurements; (B) Magnified image of the wear region showing the ploughing action of the nanodiamond particles on the WC grains.

Table 4: Comparison of the wear rate of nanocomposite coatings (15% nanodiamond) sintered at 711 and 821 ^{o}C and their respective pin-on-disc balls.

Microwave Plasma Sintering Temperature of Coatings (^{o}C)	Wear Rate (mm^{3}/Nm) (x10^{-6})	
	Nanocomposite Coating	Pin-on-disc WC Ball
711	7.90	9.32
821	5.76	9.02

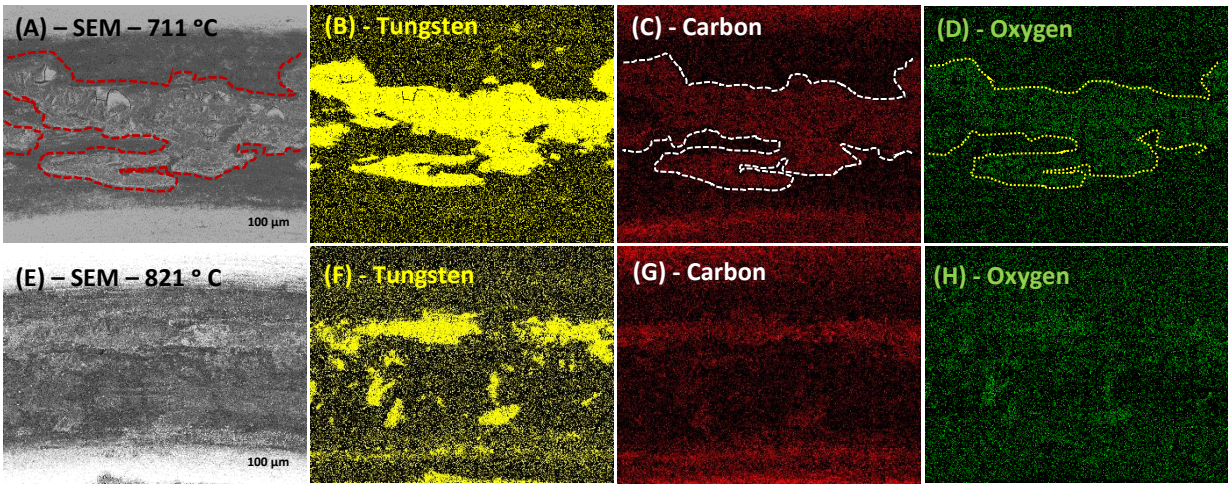

Figure 17: SEM and EDX elemental maps of the wear track of coatings sintered at 711 (A-D) and 821 °C (E-H). The nanodiamond concentration in both coatings is 15%.

Examination of the wear tracks of coatings sintered at 711 and 821 °C indicated that the transfer layers found on the wear tracks were composed of complex W-rich oxide scale containing carbon (Fig. 17). It is possible for W and W_2C to be formed during oxidation reaction of carbon [54], which would account for the W and C-rich debris. The Raman spectra of the transfer layer on the worn nanocomposite coating as shown in Fig. 17 exhibit bands in the range of 697 to 964 cm^{-1} (Fig. 18), which indicates the presence of tungsten oxide clusters and M_xO_4 [55–59]. The presence of the two oxide phases and the blue-shifted frequency indicate the distribution of significantly distorted WO_6 units in the structure [55,56]. The bands at 1332 and 1592 are consistent with nanodiamond Raman bands as discussed in section 3.4. Outside the transfer layer region, less oxidation was observed (Fig. 18).

It is concluded from this study that the general wear is a combination of abrasive, adhesive and oxidative modes. The wear mechanism of both the coating and WC balls is a result of a combination of two-body (run-in stage) and three-body (steady state stage) modes of wear,

which occur when particles are constrained initially and then are free to roll and slide without constraint after fracture [60–62].

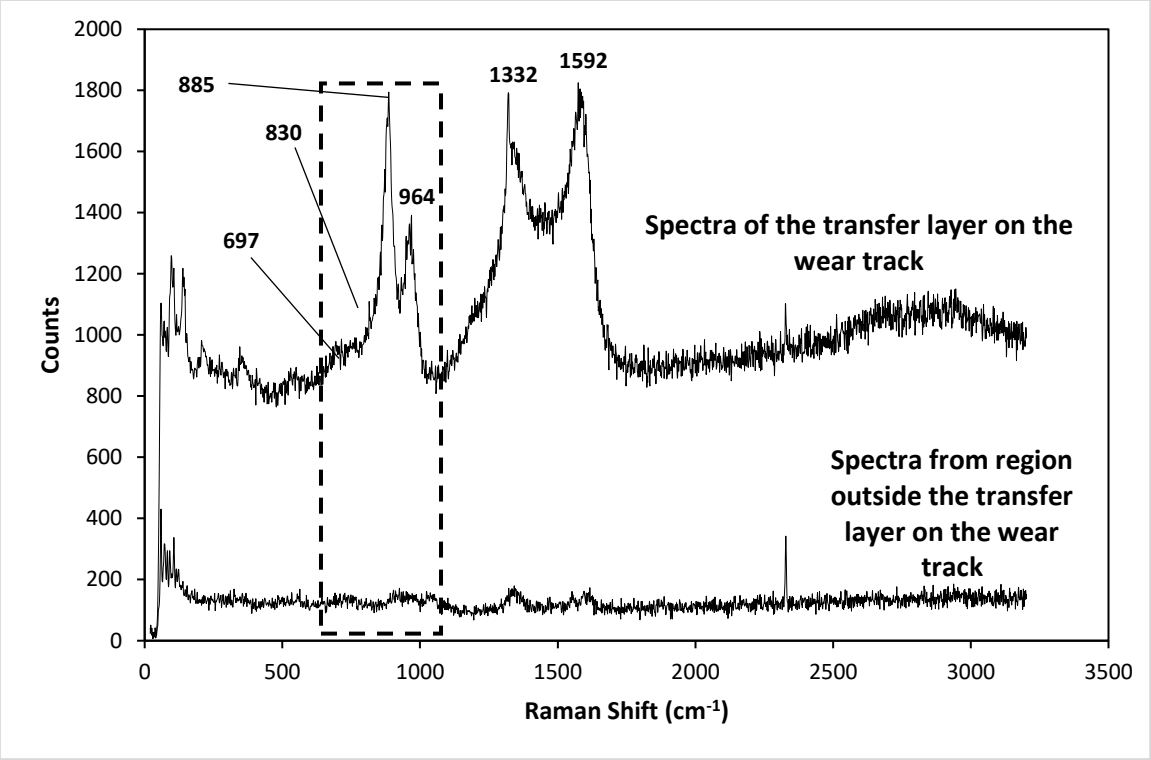

Figure 18: Raman Spectra of transfer layer on the wear track and the region on the wear track outside the transfer layer on the nanocomposite coating. The nanodiamond concentration of the coating is 15%.

4. Conclusions

In this paper, a range of wear-resistant nickel-diamond nanocomposite coatings were fabricated using a two-step approach. This involved the spray deposition of a nickel and diamond nanoparticle suspension onto stainless steel substrates using a nebuliser and the subsequent sintering in a microwave plasma system. The spray-deposited and sintered nickel-diamond nanocomposite coatings were homogenous and well adherent (HF 1). In order to optimise the performance of the deposited coatings the following parameters were evaluated: microwave plasma sintering temperature, spray duration and nanodiamond concentration. The coating evaluation was based on the morphology, adhesion and pin on disc wear performance. Based on this evaluation, it was concluded that:

- The stability of nickel-diamond nanoparticle suspension was dependent on the kind of solvent used and the concentration of nanodiamond particles in the suspension. Suspensions containing 5 to 10% nanodiamond particles in isopropanol were mostly unstable whereas at higher concentrations, they remained stable up to several months.
- The morphology of the sintered coating at lower temperatures exhibited a 'fibrous-like' structure, which gradually changed to granular structure with increasing sintering temperature.
- The roughness and thickness of the coatings generally decreased with increasing sintering temperature. Increasing the nanodiamond concentration to more than 15% also led to an increased roughness and thickness.
- The addition of nanodiamonds to the nickel yielded a significantly enhanced wear performance (126-fold improvement). Of the parameters studied, the nanodiamond concentration was the dominant parameter controlling both coating and pin-on-disc ball wear rates.

It is concluded from the study that the use of spray-deposited nickel-diamond nanoparticle suspensions combined with microwave plasma sintering provides a novel route for the application of wear resistant composite coatings onto metallic substrates.

Acknowledgements

This work was partially supported under the SFI funded I-Form Advanced Manufacturing Research Centre (16/RC/3872). The authors gratefully acknowledge the help of Assoc. Prof. Aoife Gowen (UCD SIRG) in setting up the system used for the Raman spectroscopy measurements.

References

[1] B. Cai, Y. Tan, Y. Tu, X. Wang, H. Tan, Tribological properties of Ni-base alloy composite coating modified by both graphite and TiC particles, Trans. Nonferrous Met. Soc. China. 21 (2011) 2426–2432. doi:10.1016/S1003-6326(11)61031-5.

[2] C.C. Hung, C.C. Lin, H.C. Shih, Tribological studies of electroless nickel/diamond composite coatings on steels, Diam. Relat. Mater. 17 (2008) 853–859. doi:10.1016/J.DIAMOND.2007.12.055.

[3] K. Van Acker, D. Vanhoyweghen, R. Persoons, J. Vangrunderbeek, Influence of tungsten carbide particle size and distribution on the wear resistance of laser clad WC/Ni coatings, Wear. 258 (2005) 194–202. doi:10.1016/J.WEAR.2004.09.041.

[4] H. Gül, F. Kılıç, M. Uysal, S. Aslan, A. Alp, H. Akbulut, Effect of particle concentration on the structure and tribological properties of submicron particle SiC reinforced Ni metal matrix composite (MMC) coatings produced by electrodeposition, Appl. Surf. Sci. 258 (2012) 4260–4267. doi:10.1016/J.APSUSC.2011.12.069.

[5] S. Karthikeyan, L. Vijayaraghavan, Influence of Nano Al2O3 Particles on the Adhesion, Hardness and Wear Resistance of Electroless NiP Coatings, Int. J. Mater. Mech. Manuf. 4 (2015) 106–110. doi:10.7763/IJMMM.2016.V4.234.

[6] X. Zhang, J. Qin, M.K. Das, R. Hao, H. Zhong, A. Thueploy, S. Limpanart, Y. Boonyongmaneerat, M. Ma, R. Liu, Co-electrodeposition of hard Ni-W/diamond nanocomposite coatings, Sci. Rep. 6 (2016) 22285. doi:10.1038/srep22285.

[7] J. Wang, F.-L. Zhang, T. Zhang, W.-G. Liu, W.-X. Li, Y.-M. Zhou, Preparation of Ni-P-diamond coatings with dry friction characteristics and abrasive wear resistance, Int. J. Refract. Met. Hard Mater. 70 (2018) 32–38. doi:10.1016/J.IJRMHM.2017.09.012.

[8] N.K. Shrestha, T. Takebe, T. Saji, Effect of particle size on the co-deposition of

diamond with nickel in presence of a redox-active surfactant and mechanical property of the coatings, Diam. Relat. Mater. 15 (2006) 1570–1575. doi:10.1016/J.DIAMOND.2005.12.040.

[9] B. Bozzini, M. Boniardi, A. Fanigliulo, F. Bogani, Tribological properties of electroless Ni-P/diamond composite films, Mater. Res. Bull. 36 (2001) 1889–1902. doi:10.1016/S0025-5408(01)00672-9.

[10] L. Wang, Y. Gao, Q. Xue, H. Liu, T. Xu, Effects of nano-diamond particles on the structure and tribological property of Ni-matrix nanocomposite coatings, Mater. Sci. Eng. A. 390 (2005) 313–318. doi:10.1016/J.MSEA.2004.08.033.

[11] I.A. Ibrahim, F.A. Mohamed, E.J. Lavernia, Particulate reinforced metal matrix composites - a review, J. Mater. Sci. 26 (1991) 1137–1156. doi:10.1007/BF00544448.

[12] M. Petrova, Z. Noncheva, E. Dobreva, Electroless deposition of diamond powder dispersed nickel–phosphorus coatings on steel substrate, Trans. IMF. 89 (2011) 89–94. doi:10.1179/174591911X12971865404438.

[13] V.V.. Reddy, B. Ramamoorthy, P.K. Nair, A study on the wear resistance of electroless Ni–P/Diamond composite coatings, Wear. 239 (2000) 111–116. doi:10.1016/S0043-1648(00)00330-6.

[14] H. Mazaheri, S.R. Allahkaram, Deposition, characterization and electrochemical evaluation of Ni–P–nano diamond composite coatings, Appl. Surf. Sci. 258 (2012) 4574–4580. doi:10.1016/J.APSUSC.2012.01.031.

[15] H. Xu, Z. Yang, M.-K. Li, Y.-L. Shi, Y. Huang, H.-L. Li, Synthesis and properties of electroless Ni–P–Nanometer Diamond composite coatings, Surf. Coatings Technol. 191 (2005) 161–165. doi:10.1016/J.SURFCOAT.2004.03.045.

[16] V.N. Mochalin, O. Shenderova, D. Ho, Y. Gogotsi, The properties and applications of

nanodiamonds, Nat. Nanotechnol. 7 (2012) 11–23. doi:10.1038/nnano.2011.209.

[17] Y. Zhang, K.Y. Rhee, D. Hui, S.-J. Park, A critical review of nanodiamond based nanocomposites: Synthesis, properties and applications, Compos. Part B Eng. 143 (2018) 19–27. doi:10.1016/J.COMPOSITESB.2018.01.028.

[18] J.G. Buijnsters, P. Shankar, J.J. Ter Meulen, Direct deposition of polycrystalline diamond onto steel substrates, Surf. Coatings Technol. 201 (2007) 8955–8960. doi:10.1016/J.SURFCOAT.2007.04.012.

[19] Y.S. Li, Y. Tang, Q. Yang, C. Xiao, A. Hirose, Growth and adhesion failure of diamond thin films deposited on stainless steel with ultra-thin dual metal interlayers, Appl. Surf. Sci. 256 (2010) 7653–7657. doi:10.1016/J.APSUSC.2010.06.022.

[20] J.G. Buijnsters, P. Shankar, W.J.P. van Enckevort, J.J. Schermer, J.J. ter Meulen, The adhesion of hot-filament CVD diamond films on AISI type 316 austenitic stainless steel, Diam. Relat. Mater. 13 (2004) 848–857. doi:10.1016/J.DIAMOND.2003.11.012.

[21] D. Damm, A. Contin, F. Barbieri, V. Trava-Airoldi, D. Barquete, E. Corat, D.D. Damm, A. Contin, F.C. Barbieri, V.J. Trava-Airoldi, D.M. Barquete, E.J. Corat, Interlayers Applied to CVD Diamond Deposition on Steel Substrate: A Review, Coatings. 7 (2017) 141. doi:10.3390/coatings7090141.

[22] I. Endler, A. Leonhardt, H.-J. Scheibe, R. Born, Interlayers for diamond deposition on tool materials, Diam. Relat. Mater. 5 (1996) 299–303. doi:10.1016/0925-9635(95)00352-5.

[23] X. Li, J. Ye, H. Zhang, T. Feng, J. Chen, X. Hu, Sandblasting induced stress release and enhanced adhesion strength of diamond films deposited on austenite stainless steel, Appl. Surf. Sci. 412 (2017) 366–373. doi:10.1016/J.APSUSC.2017.03.214.

[24] Y.S. Li, Y. Tang, Q. Yang, J. Maley, R. Sammynaiken, T. Regier, C. Xiao, A. Hirose,

Ultrathin W−Al Dual Interlayer Approach to Depositing Smooth and Adherent Nanocrystalline Diamond Films on Stainless Steel, ACS Appl. Mater. Interfaces. 2 (2010) 335–338. doi:10.1021/am9007159.

[25] J.G. Buijnsters, P. Shankar, W. Fleischer, W.J.P. van Enckevort, J.J. Schermer, J.J. ter Meulen, CVD diamond deposition on steel using arc-plated chromium nitride interlayers, Diam. Relat. Mater. 11 (2002) 536–544. doi:10.1016/S0925-9635(01)00628-8.

[26] J. Halme, J. Saarinen, P. Lund, Spray deposition and compression of TiO2 nanoparticle films for dye-sensitized solar cells on plastic substrates, Sol. Energy Mater. Sol. Cells. 90 (2006) 887–899. doi:10.1016/J.SOLMAT.2005.05.013.

[27] M. Awais, E. Gibson, J.G. Vos, D.P. Dowling, A. Hagfeldt, D. Dini, Fabrication of Efficient NiO Photocathodes Prepared via RDS with Novel Routes of Substrate Processing for *p* -Type Dye-Sensitized Solar Cells, ChemElectroChem. 1 (2014) 384–391. doi:10.1002/celc.201300178.

[28] M. Awais, D.D. Dowling, F. Decker, D. Dini, Photoelectrochemical properties of mesoporous NiO x deposited on technical FTO via nanopowder sintering in conventional and plasma atmospheres, Springerplus. 4 (2015) 564. doi:10.1186/s40064-015-1265-3.

[29] E.J. Ekoi, M. Awais, D.P. Dowling, Microwave Plasmas as a Processing Tool for Tailoring the Surface Properties of Ceramic Coatings, in: Recent Adv. Porous Ceram., InTech, 2018. doi:10.5772/intechopen.71686.

[30] A.S.T.. Standard, Standard Test Method for Wear Testing with a Pin-on-Disk Apparatus 1, West Conshohocken, PA, 2006.

[31] T. Wang, S. Handschuh-Wang, P. Qin, Y. Yang, X. Zhou, Y. Tang, Enhancing the

colloidal stability of detonation synthesized diamond particles in aqueous solutions by adsorbing organic mono-, bi- and tridentate molecules, J. Colloid Interface Sci. 499 (2017) 102–109. doi:10.1016/J.JCIS.2017.03.065.

[32] N. Gibson, O. Shenderova, T.J.M. Luo, S. Moseenkov, V. Bondar, A. Puzyr, K. Purtov, Z. Fitzgerald, D.W. Brenner, Colloidal stability of modified nanodiamond particles, Diam. Relat. Mater. 18 (2009) 620–626. doi:10.1016/J.DIAMOND.2008.10.049.

[33] X. Xu, Z. Yu, Y. Zhu, B. Wang, Effect of sodium oleate adsorption on the colloidal stability and zeta potential of detonation synthesized diamond particles in aqueous solutions, Diam. Relat. Mater. 14 (2005) 206–212. doi:10.1016/J.DIAMOND.2004.11.004.

[34] O. Shenderova, S. Hens, G. McGuire, Seeding slurries based on detonation nanodiamond in DMSO, Diam. Relat. Mater. 19 (2010) 260–267. doi:10.1016/J.DIAMOND.2009.10.008.

[35] C.-C. Li, C.-L. Huang, Preparation of clear colloidal solutions of detonation nanodiamond in organic solvents, Colloids Surfaces A Physicochem. Eng. Asp. 353 (2010) 52–56. doi:10.1016/J.COLSURFA.2009.10.019.

[36] M. Rahimian, N. Ehsani, N. Parvin, H. reza Baharvandi, The effect of particle size, sintering temperature and sintering time on the properties of Al–Al2O3 composites, made by powder metallurgy, J. Mater. Process. Technol. 209 (2009) 5387–5393. doi:10.1016/J.JMATPROTEC.2009.04.007.

[37] V.I. Korepanov, H. Hamaguchi, E. Osawa, V. Ermolenkov, I.K. Lednev, B.J.M. Etzold, O. Levinson, B. Zousman, C.P. Epperla, H.-C. Chang, Carbon structure in nanodiamonds elucidated from Raman spectroscopy, Carbon N. Y. 121 (2017) 322–

329. doi:10.1016/J.CARBON.2017.06.012.

[38] J. Hodkiewicz, Characterizing Carbon Materials with Raman Spectroscopy, Madison, WI, 2010. https://assets.thermofisher.com/TFS-Assets/CAD/Application-Notes/D19504~.pdf (accessed January 7, 2019).

[39] J.G. Buijnsters, P. Shankar, P. Gopalakrishnan, W.J.P. van Enckevort, J.J. Schermer, S.S. Ramakrishnan, J.J. ter Meulen, Diffusion-modified boride interlayers for chemical vapour deposition of low-residual-stress diamond films on steel substrates, Thin Solid Films. 426 (2003) 85–93. doi:10.1016/S0040-6090(03)00013-0.

[40] N.G. Ferreira, E. Abramof, N.F. Leite, E.J. Corat, V.J. Trava-Airoldi, Analysis of residual stress in diamond films by x-ray diffraction and micro-Raman spectroscopy, J. Appl. Phys. 91 (2002) 2466–2472. doi:10.1063/1.1431431.

[41] L. Chandra, M. Chhowalla, G.A.J. Amaratunga, T.W. Clyne, Residual stresses and debonding of diamond films on titanium alloy substrates, Diam. Relat. Mater. 5 (1996) 674–681. doi:10.1016/0925-9635(95)00431-9.

[42] J.G. Kim, J. Yu, Behavior of residual stress on CVD diamond films, Mater. Sci. Eng. B. 57 (1998) 24–27. doi:10.1016/S0921-5107(98)00215-3.

[43] N. Vidakis, A. Antoniadis, N. Bilalis, The VDI 3198 indentation test evaluation of a reliable qualitative control for layered compounds, J. Mater. Process. Technol. 143–144 (2003) 481–485. doi:10.1016/S0924-0136(03)00300-5.

[44] W. Heinke, A. Leyland, A. Matthews, G. Berg, C. Friedrich, E. Broszeit, Evaluation of PVD nitride coatings, using impact, scratch and Rockwell-C adhesion tests, Thin Solid Films. 270 (1995) 431–438. doi:10.1016/0040-6090(95)06934-8.

[45] Y.-J. Xue, X.-Z. Jia, Y.-W. Zhou, W. Ma, J.-S. Li, Tribological performance of Ni–CeO2 composite coatings by electrodeposition, Surf. Coatings Technol. 200 (2006)

5677–5681. doi:10.1016/J.SURFCOAT.2005.08.002.

[46] B. Müller, H. Ferkel, Al2O3-nanoparticle distribution in plated nickel composite films, Nanostructured Mater. 10 (1998) 1285–1288. doi:10.1016/S0965-9773(99)00008-2.

[47] K.. Hou, M.. Ger, L.. Wang, S.. Ke, The wear behaviour of electro-codeposited Ni–SiC composites, Wear. 253 (2002) 994–1003. doi:10.1016/S0043-1648(02)00222-3.

[48] N. Kumar, G. Natarajan, R. Dumpala, R. Pandian, A. Bahuguna, S.K. Srivastava, T.R. Ravindran, S. Rajagopalan, S. Dash, A.K. Tyagi, M.S. Ramachandra Rao, Microstructure and phase composition dependent tribological properties of TiC/a-C nanocomposite thin films, Surf. Coatings Technol. 258 (2014) 557–565. doi:10.1016/J.SURFCOAT.2014.08.038.

[49] K.L. Johnson, Contact mechanics and the wear of metals, Wear. 190 (1995) 162–170. doi:10.1016/0043-1648(95)06665-9.

[50] D.A. Rigney, L.H. Chen, M.G.S. Naylor, A.R. Rosenfield, Wear processes in sliding systems, Wear. 100 (1984) 195–219. doi:10.1016/0043-1648(84)90013-9.

[51] D.K. Dwivedi, Adhesive wear behaviour of cast aluminium–silicon alloys: Overview, Mater. Des. 31 (2010) 2517–2531. doi:10.1016/J.MATDES.2009.11.038.

[52] N.P. Suh, An overview of the delamination theory of wear, Wear. 44 (1977) 1–16. doi:10.1016/0043-1648(77)90081-3.

[53] H. Gül, M. Uysal, H. Akbulut, A. Alp, Effect of PC electrodeposition on the structure and tribological behavior of Ni–Al2O3 nanocomposite coatings, Surf. Coatings Technol. 258 (2014) 1202–1211. doi:10.1016/J.SURFCOAT.2014.07.002.

[54] V.B. Voitovich, V.V. Sverdel, R.F. Voitovich, E.I. Golovko, Oxidation of WC-Co, WC-Ni and WC-Co-Ni hard metals in the temperature range 500–800 °C, Int. J. Refract. Met. Hard Mater. 14 (1996) 289–295. doi:10.1016/0263-4368(96)00009-1.

[55] E.I.R.-M. and, I.E. Wachs*, Structural Determination of Bulk and Surface Tungsten Oxides with UV−vis Diffuse Reflectance Spectroscopy and Raman Spectroscopy, (2007). doi:10.1021/JP074219C.

[56] F.D. Hardcastle, I.E. Wachs, Determination of the molecular structures of tungstates by Raman spectroscopy, J. Raman Spectrosc. 26 (1995) 397–405. doi:10.1002/jrs.1250260603.

[57] M. Aristizabal, L.C. Ardila, F. Veiga, M. Arizmendi, J. Fernandez, J.M. Sánchez, Comparison of the friction and wear behaviour of WC–Ni–Co–Cr and WC–Co hardmetals in contact with steel at high temperatures, Wear. 280–281 (2012) 15–21. doi:10.1016/J.WEAR.2012.01.015.

[58] S. Huang, J. Xiong, Z. Guo, W. Wan, L. Tang, H. Zhong, W. Zhou, B. Wang, Oxidation of WC-TiC-TaC-Co hard materials at relatively low temperature, Int. J. Refract. Met. Hard Mater. 48 (2015) 134–140. doi:10.1016/J.IJRMHM.2014.08.002.

[59] L. Chen, D. Yi, B. Wang, H. Liu, C. Wu, Mechanism of the early stages of oxidation of WC–Co cemented carbides, Corros. Sci. 103 (2016) 75–87. doi:10.1016/J.CORSCI.2015.11.007.

[60] L. Wu, X. Guo, J. Zhang, L. Wu, X. Guo, J. Zhang, Abrasive Resistant Coatings—A Review, Lubricants. 2 (2014) 66–89. doi:10.3390/lubricants2020066.

[61] R.M. Gresham, ASM HANDBOOK Volume 18: Friction, Lubrication, and Wear Technology, Society of Tribologists and Lubrication Engineers, Park Ridge, 2018.

[62] J.D. Gates, Two-body and three-body abrasion: A critical discussion, Wear. 214 (1998) 139–146. doi:10.1016/S0043-1648(97)00188-9.